arXiv:1611.10062v1 [cond-mat.supr-con] 30 Nov 2016

Optical properties of the optimally doped $Ca_{8.5}La_{1.5}(Pt_3As_8)(Fe_2As_2)_5$ single crystal

Yu-il Seo[1], Woo-Jae Choi[1], Shin-ich Kimura[2], Yunkyu Bang[3],* and Yong Seung Kwon[1]†
[1]*Department of Emerging Materials Science, Daegu Gyeongbuk Institute of Science and Technology (DGIST), Daegu 711-873, Republic of Korea*
[2]*FBS and Department of Physics, Osaka University, Suita 565-0871, Japan*
[3]*Department of Physics, Chonnam National University, Kwangju 500-757, Republic of Korea*
(Dated: December 1, 2016)

We have measured the reflectivity of the optimally doped $Ca_{8.5}La_{1.5}(Pt_3As_8)(Fe_{10}As_{10})$ single crystal (T_c = 32.8K) over the broad frequency range from 40 to 12000 cm^{-1} and for temperatures from 8 to 300 K. The optical conductivity spectra of the low frequency region ($< 1,000\ cm^{-1}$) in the normal state (80 K $< T \leq$ 300 K) is well fitted with two Drude forms, which indicates the presence of multiple bands at the Fermi level. Decreasing temperature below 80 K, this low frequency Drude spectra develops pseudogap (PG) hump structure at around $\approx 100\ cm^{-1}$ and continuously evolves into the fully opened superconducting (SC) gap structure below T_c. Theoretical calculations of the optical conductivity with the preformed Cooper pair model provide an excellent description of the temperature evolution of the PG structure above T_c into the SC gap structure below T_c. The extracted two SC gap sizes are Δ_S = 4.9 *meV* and Δ_L = 14.2 *meV*, identifying $Ca_{8.5}La_{1.5}(Pt_3As_8)(Fe_{10}As_{10})$ as a strong coupling multiple gap superconductor.

PACS numbers: 74.25.nd,74.20.Rp,74.70.Xa

I. INTRODUCTION

Recently discovered Fe-pnictide compounds, $Ca_{10}(Pt_3As_8)(Fe_2As_2)_5$ (so-called 10-3-8 compound) and $Ca_{10}(Pt_4As_8)(Fe_2As_2)_5$ (so-called 10-4-8 compound) [1–4], added another new class to the family of the Fe-based superconductors (IBSs). They are showing the prototype behavior of the subtle balance and competition between magnetism and superconductivity commonly observed in other IBSs. Both compounds share similar overall crystal structure, consisting of tetrahedral FeAs planes sandwiched between the planar Pt_nAs_8 ($n = 3,4$) intermediary layers. However, in fine details, there exist also distinct differences between them.

The parent 10-4-8 compound has a tetragonal crystal structure and is metallic. It becomes superconducting (SC) without doping with the maximum T_c of $\sim$ 38 K [1, 5], and doping of electrons only suppresses the SC transition temperature[4, 6, 7]. On the other hand, the parent 10-3-8 compound has a triclinic crystal structure and is semiconducting. This compound becomes antiferromagnetically ordered below $T_N \approx 120$ K without any further reduction in the crystal symmetry [6]. Superconductivity can be induced by doping of electrons: for instance, La substitution at the Ca site, or Pt substitution at the Fe site [6]. The maximum T_c for each substitution can be $\sim$ 32 K and $\sim$ 15 K, respectively [6].

The band structure calculations[8] suggested that these differences arise from the increased metallicity of the PtAs layers. And recent angle resolved photoemission spectroscopy (ARPES) experiment further suggested that this difference between two compounds could be developed by the number of the band-edge singularities [9]. In order to study this subtle relation between the electronic structure and superconductivity in these materials, various experiments have already been performed: such as transport [10], pressure effect [11], ARPES [12], magnetic force microscope (MFM) [13], upper critical field (H_{c2}) [14], nuclear magnetic resonance (NMR) [15], and penetration depth $\lambda(T)$[16] measurements, etc. However, the IR spectroscopy experiment has not yet been carried out with these compounds. This technique is particularly a useful tool to directly study the low energy dynamics of the correlated materials with temperature variation, and, therefore, it is able to investigate the systematic development of superconductivity with temperature and any non-trivial evolution of the correlation effects, if exists.

In this paper, we have measured the IR reflectivity and analyzed the optical properties of the optimally La-doped 10-3-8 compound, $Ca_{8.5}La_{1.5}(Pt_3As_8)(Fe_2As_2)_5$ single crystal ($T_c \approx$32.8 K). In view of the phase diagram with electron doping of the previous study[10], our compound is located far apart from the antiferromagnetic (AFM) quantum critical point (QCP) where T_N goes to zero in the phase diagram. However, we speculate that our compound is located near another QCP in the universal phase diagram, from the observations of (1) the maximum T_c with doping variation, and (2) the T-linear resistivity data above T_c up to 300 K. It is interesting to note that these QCP behaviors far away from the AFM QCP are similar to the case of the cuprate superconductors. Then, most interestingly, we have also found the pseudogap (PG) behavior in the optical conductivity of our sample up to the temperature about three times higher ($\sim$ 80 K) than $T_c(\approx$ 33 K). With the observation that our compound is far away from the AFM QCP, it is logical to conclude that the PG behavior of the optimal doped 10-3-8 compound is not related to the AFM correlation. We have employed the preformed Cooper pair model to calculate the real part of the optical conductivity $\sigma(\omega, T)$ and successfully reproduced the PG feature far above T_c and its consistent evolution to the SC gap structure below T_c.

*ykbang@chonnam.ac.kr
†yskwon@dgist.ac.kr

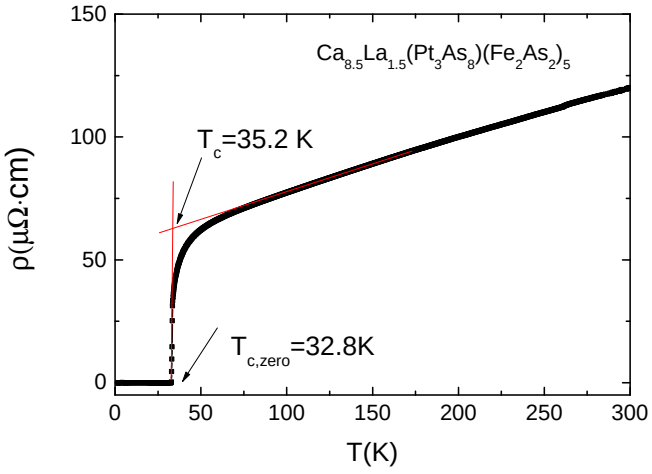

FIG. 1: (Color online) Temperature dependence of the DC electrical resistivity $\rho(T)$ of the $Ca_{8.5}La_{1.5}(Pt_3As_8)(Fe_2As_2)_5$ single crystal.

Combining the previous reports of the PG observations in several IBS compounds and cuprate superconductors, our observation establishes that the PG phenomena induced by a SC correlation is a generic phenomena of the strongly correlated unconventional superconductors.

II. EXPERIMENTAL DETAILS

High quality single crystals of $Ca_{8.5}La_{1.5}(Pt_3As_8)(Fe_2As_2)_5$ were grown by a Bridgeman method with a sealed molybdenum crucible at 1250° C. Before performing the Bridgeman method, we made the precursors of CaAs, LaAs and FeAs in advance. Figure 1 shows the in-plane electrical resistivity $\rho(T)$ of the $Ca_{8.5}La_{1.5}(Pt_3As_8)(Fe_2As_2)_5$ single crystal. We do not see any noticeable anomaly in $\rho(T)$ around $T_N^0 \approx 120$ K (the Neel temperature of the undoped parent 10-3-8 compound) and below due to the spin density wave (SDW) transition. The SC transition begins at T_c=35.2 K and zero resistivity occurs at $T_{c,zero} = 32.8$ K, respectively. These transition temperatures are about 7-9 K higher than the one with similar nominal doping of La ($x = 1.45$) in the previously reported work [10], indicating that our sample is a substantially higher quality single crystal.

Another noticeable feature is that $\rho(T)$ shows the T-linear temperature dependence above T_c up to 300 K. This linear-in-T behavior in $\rho(T)$ is commonly observed in other optimally doped IBSs [17–20] and is a signature that the sample is near the QCP. This is consistent with the phase diagram of Ref.[10], where the maximum SC T_c was also located with the La doping "x_{max}^{sc}" ≈ 1.5. Moreover the phase diagram of Ref.[10] shows that the magnetic critical doping "x_c^{mag}", where $T_N \rightarrow 0$, is near ≈ 0.3, which is far apart from the optimal doping x_{max}^{sc} for the maximum SC T_c. Therefore, in view of the phase diagram of Ref.[10] and our result, we speculate that there exist two QCPs in the La-doped 10-8-3 compound: one is the QCP due to magnetic fluctuations where $T_N \rightarrow 0$, and the other is the QCP due to unknown quantum fluctuations where the SC T_c becomes maximum. The former type of QCP is more common with many IBSs as well as most of heavy fermion superconductors, while the latter type of QCP is well represented in the high-T_c cuprate superconductors. Therefore, clarifying the nature of the QCP in the 10-3-8 compound will be particularly interesting in connection with the mystery of the high-T_c cuprate superconductors.

In order to investigate the electronic structure as well as the SC properties of $Ca_{8.5}La_{1.5}(Pt_3As_8)(Fe_2As_2)_5$, we have measured the optical reflectivity $R(\omega,T)$ of this single crystal in a broad frequency range from 40 to 12000 cm^{-1} and for various temperatures from 8 to 300 K. We used a Michelson-type rapid-scan Fourier spectrometer (Jasco FTIR610). In particular, we used a specially designed feedback positioning system to drastically reduce the overall uncertainty level. The uncertainty of our data was maintained less than 0.5%. For more details of experimental methods of reference setting and control of data uncertainty, we refer to our previous paper[21].

III. RESULTS AND DISCUSSIONS

A. Reflectivity and Optical Conductivity

Figure 2 shows the reflectivity spectra $R(\omega,T)$ of $Ca_{8.5}La_{1.5}(Pt_3As_8)(Fe_2As_2)_5$ single crystal at several different temperatures from 8 K to 300 K. The main panel shows the full measured data for frequencies from 50 cm^{-1} to 12000 cm^{-1} in log scale, and the inset shows the close-up view of the data from 0 cm^{-1} to 600 cm^{-1} in linear scale; here the data from 0 cm^{-1} to 40 cm^{-1} are not the measured ones but extrapolated ones as explained below.

In the normal state (the data sets for $T \geq 40$ K), $R(\omega)$ approaches to unity at zero frequency and increases as decreasing temperature in far-infrared region, showing a typical metallic behavior of $Ca_{8.5}La_{1.5}(Pt_3As_8)(Fe_2As_2)_5$. On entering the SC phase (the data sets below 40 K), the low frequency reflectivity turns up quickly, and reaches the flat unity response below $\sim$80 cm^{-1} reflecting the SC gap opening. As the temperature increases toward T_c the flat unity response shrinks to the lower frequency region as the SC gap size is decreasing. The shape of the flat part in $R(\omega)$ at low frequencies and its temperature dependence are clear signatures of the fully opened SC gap. However, the most interesting development of the reflectivity spectra in Fig.2 occurs in the data sets for 80 K (cyan color) and 40 K (purple color), which are still in the normal state. Both data sets show a curious suppression of spectra in the low frequency region around 100 cm^{-1} (see the inset of Fig.2).

For more convenient analysis, we converted our reflectivity data $R(\omega)$ into the real part of the optical conductivity $\sigma_1(\omega)$ by the Kramers-Kronig (KK) transformation. For extrapolation of the data for the KK-transformation, at low frequencies, we used the Hagen-Rubens extrapolation formula for the nor-

mal state and the form $(1 - A\omega^4)$ below the gap in the SC state. For high frequencies above 12000 cm^{-1}, the standard $1/\omega^4$ form plus a constant reflectivity are used up to 40 eV.

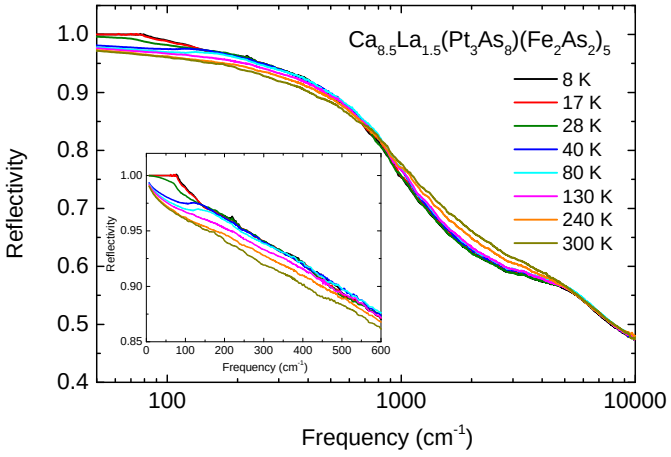

FIG. 2: (Color online) Reflectivity spectra $R(\omega)$ of the $Ca_{8.5}La_{1.5}(Pt_3As_8)(Fe_2As_2)_5$ single crystal at several temperatures. The inset shows the enlarged view of spectra below 600 cm^{-1}.

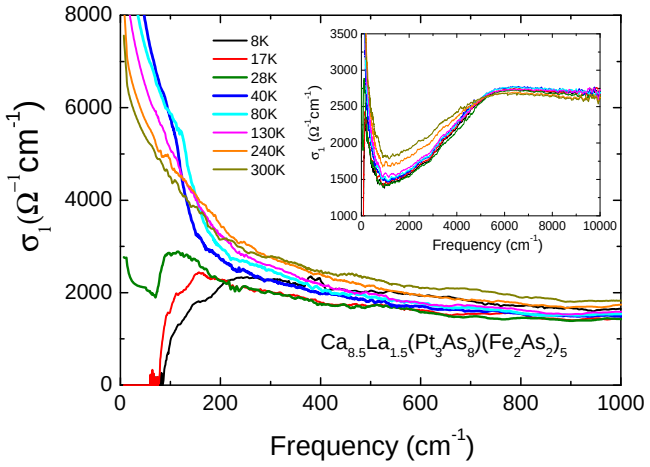

FIG. 3: (Color online) Real part of optical conductivity $\sigma_1(\omega)$ of $Ca_{8.5}La_{1.5}(Pt_3As_8)(Fe_2As_2)_5$ single crystal for 8, 17, 28, 40, 80, 130, 180, 240, and 300 K, respectively. The inset shows the same data $\sigma_1(\omega)$ in wider view up to 10,000 cm^{-1}.

Figure 3 shows these results of $\sigma_1(\omega)$, obtained from the data of Fig.2, in the frequency range from 0 to 1000 cm^{-1} for various temperatures. The optical conductivity spectra at 130, 240 and 300 K – which are in normal state – show a very broad Drude peak centered at $\omega = 0$ and then monotonically decrease until the interband transition starts appearing around 1000 cm^{-1} (see the inset of Fig.3). The interband transition spectra continues to form a broad hump around 6000 cm^{-1}, which is almost independent of temperatures.

As the temperature decreases down to 80 K (cyan color) and 40 K (blue color) – which are still in normal state by transport/thermodynamic measurements – (1) the Drude part of spectra rapidly sharpens, and then (2) a peculiar hump structure around 80-150 cm^{-1} appears on top of the smooth Drude spectra. The former is the expected evolution due to the formation of coherent quasiparticles as temperature decreases. The striking feature is the latter, namely, the appearance of the shoulder-like hump structure far above T_c on top of the Drude response in the frequency range of 80-150 cm^{-1}, indicating an incomplete gap – hence called PG – formation over the Fermi surfaces or in a part of the Fermi surfaces. Then below T_c, i.e., at 28 K, 17 K and 8 K, $\sigma_1(\omega)$ shows a clean opening of the SC energy gap with the absorption edge at about 80 cm^{-1} and a peak position at around 150 cm^{-1}. Comparing this SC gap structure at around 80-150 cm^{-1} below T_c, the hump structure around 80-150 cm^{-1}, above T_c at 40 K and 80 K, appears to be a continuous evolution of the SC correlation below T_c.

The observation of the PG features in the IBSs with the optical spectroscopy measurements is now quite common. For example, the underdoped ($x \approx 0.12, 0.2$) [22] and the slightly underdoped ($x \approx 0.3$) [21] $Ba_{1-x}K_xFe_2As_2$ have reported the similar behavior in their optical measurements: namely, the hump structures in the optical conductivity $\sigma_1(\omega)$ above T_c (about three times of T_c for all cases) in the same energy scale as the SC gap energy, and their continuous evolution into the SC gap. These authors concluded that this hump structure is not related with a magnetic correlation but rather connected to the SC gap, hence possibly a precursor of the preformed Cooper pairs. The optimally Co-doped $Ba(Fe_{0.92}Co_{0.08})As_2$[23] also has shown a similar hump structure at 30 K (T_c=22.5 K) and its evolution into the SC gap below T_c; however, the authors of Ref.[23] advocated, as its origin, the impurity bound state or a low-energy interband transition, with which we do not agree.

More recently, Surmach et al. [24] have performed a comprehensive measurements of muon-spin relaxation (μSR), inelastic neutron scattering (INS), and NMR on Pt-doped $(CaFe_{1-x}Pt_xAs)_{10}Pt_3As_8$ (T_c = 13 K) – the same 10-3-8 compound we studied in this paper but with Pt doping on Fe sites. They found a PG behavior in the $1/T_1$ data of ^{75}As NMR below $T^* \approx 45$ K (about three times higher than T_c). These authors concluded from a combination of measurements of μSR, INS, together with NMR that this PG behavior is likely to be associated with the preformed Cooper pairs. Therefore, our observation of a similar PG behavior in the optimally doped $Ca_{8.5}La_{1.5}(Pt_3As_8)(Fe_2As_2)_5$ compound has strengthened the universal nature of the PG phenomena originating from the preformed Cooper pairs or a precursor effect from the SC correlation in the 10-3-8 compound.

B. Temperature Dependence of Spectral Weight Transfer

To further understand the temperature evolution of the optical conductivity shown in Fig.3, we have analyzed the temperature dependence of the "partial" spectral weight $SW(T;\omega_c)$ with different cutoffs defined as

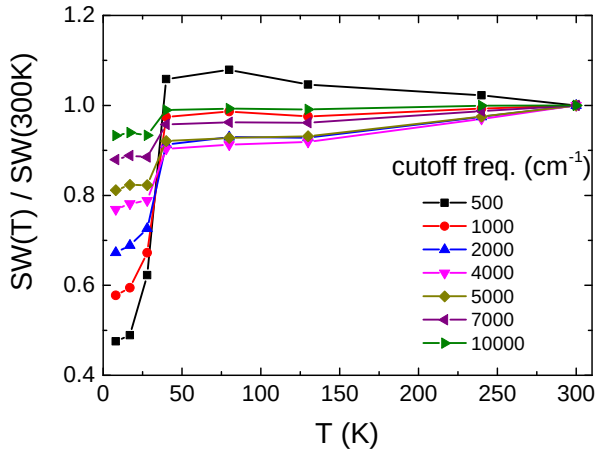

FIG. 4: (Color online) Temperature dependence of the normalized "partial" spectral weights $SW(T;\omega_c)/SW(300\ K;\omega_c)$ of the optical conductivity data in Fig.3 with different cutoff frequency ω_c: 10000 cm^{-1}, 7000 cm^{-1}, 5000 cm^{-1}, 4000 cm^{-1}, 2000 cm^{-1}, 1000 cm^{-1}, and 500 cm^{-1}, respectively.

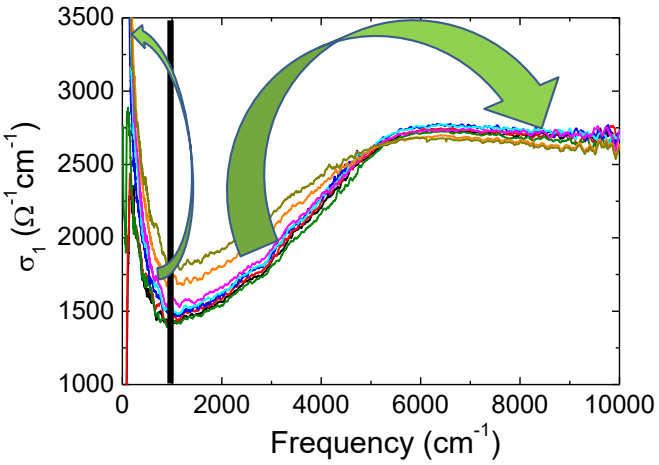

FIG. 5: (Color online) A schematic illustration of the spectral weight transfer with temperature variation. The spectral density in mid-frequency range ($\sim 500\ cm^{-1} < \omega < \sim 5{,}000\ cm^{-1}$) is continuously depleted with decreasing temperature. This depleted spectral weight is roughly divided by $\omega^* \sim 1{,}000\ cm^{-1}$ (black vertical line), and the spectral weight below ω^* and the spectral weight above ω^* are separately conserved (of course, this conservation holds only approximately).

$$SW(T;\omega_c) = \int_0^{\omega_c} \sigma_1(\omega;T)d\omega, \qquad (1)$$

where ω_c is a cutoff frequency. Figure 4 shows the results of $SW(T;\omega_c)$ that reveal non-trivial information of the correlated electron system.

The total spectral weight up to 10,000 cm^{-1} is constant on changing temperature from T_c to 300 K confirming that the sum rule is satisfied. However, with lower cutoff frequency ω_c, the sum rule is being deviated, as it should be, but in a non-trivial way. First, the normalized "partial" spectral weight $SW(T;\omega_c)/SW(300\ K;\omega_c)$ with $1{,}000\ cm^{-1} < \omega_c < 10{,}000\ cm^{-1}$ is monotonically decreasing with lowering temperature down to T_c. This means that the spectral weight below the cutoff frequency ω_c is transferred to the higher frequency region above the cutoff frequency ω_c when temperature decreases, which is an opposite behavior from a standard Drude type metallic state. Second, the rate of this spectral weight transfer is not monotonously increasing with lowering the cutoff frequency ω_c; the deceasing rate increases to the maximum when the cutoff frequency is lowered to $\omega_c = 4{,}000\ cm^{-1}$ (pink inverse triangles) and then it becomes weaker with lowering cutoff frequencies to $\omega_c = 2{,}000\ cm^{-1}$, and $1{,}000\ cm^{-1}$. Third, when $\omega_c = 1{,}000\ cm^{-1}$, the partial sum rule is "almost" recovered again: namely, the spectral weight below $\omega_c^* = 1{,}000\ cm^{-1}$ (black squares) is separately conserved with respect to the temperature variation up to T_c. Finally, when $\omega = 500\ cm^{-1} < \omega_c^*$ (black squares), the "partial" spectral weight $SW(T;\omega_c = 500\ cm^{-1})/SW(300\ K;\omega_c = 500\ cm^{-1})$ is increasing – not decreasing – with decreasing temperature.

This complicated spectral weight transfer of $SW(T;\omega_c)$ with temperature variation is summarized in Fig.5. It shows that the spectral weight transfer of $\sigma_1(\omega)$ with temperature variation is roughly divided into two parts: one part below $\omega_c^* = 1{,}000\ cm^{-1}$ and the other part above $\omega_c^* = 1{,}000\ cm^{-1}$, and each part separately conserves the spectral weight. The physical meaning of it is that the correlated electrons are divided into the low energy itinerant part (so Drude spectra) and the high energy localized part (so Lorentzian spectra). At high temperatures, a large portion of spectra in the intermediate energy range – in this particular compound, in between 500 cm^{-1} and 5000 cm^{-1} – is undetermined, hence remains incoherent. Lowering temperature, these incoherent spectra are continuously depleted and transferred either into the low frequency Drude part or into the high frequency Lorentzian part: the final fate of the incoherent spectra was actually predetermined by the frequency $\omega_c^* = 1{,}000\ cm^{-1}$ – which is the deepest valley point of the $\sigma_1(\omega)$ spectra in Fig.5 – in this particular 10-3-8 compound.

C. Drude-Lorentz model fitting for $\sigma_1^{exp}(\omega;T > T_c)$ in the normal state

We have shown that the total spectra of the normal state optical conductivity $\sigma_1(\omega)$ consists of two spectral parts – Drude part and Lorentz part – and each part conserves their spectral weights: this separate conservation of sum rule will be confirmed once more in this section. Therefore we tried to fit the data with the standard Drude-Lorentz model

$$\sigma_1(\omega) = \frac{1}{4\pi} Re\Big[\sum_j \frac{\omega_{p,j}^2}{\frac{1}{\tau_{D,j}} - i\omega} + \sum_k S_k \frac{\omega}{\frac{\omega}{\tau_{L,k}} + i(\omega_{L,k}^2 - \omega^2)}\Big] \qquad (2)$$

where $\omega_{p,j}$ and $\frac{1}{\tau_{D,j}}$ are the plasma frequency and the scattering rate for the j-th free carrier Drude band, respectively, and S_k, $\omega_{L,k}$ and $\frac{1}{\tau_{L,k}}$ are the spectral weight, the Lorentz oscillator frequency, and the scattering rate of the k-th oscillator, respectively.

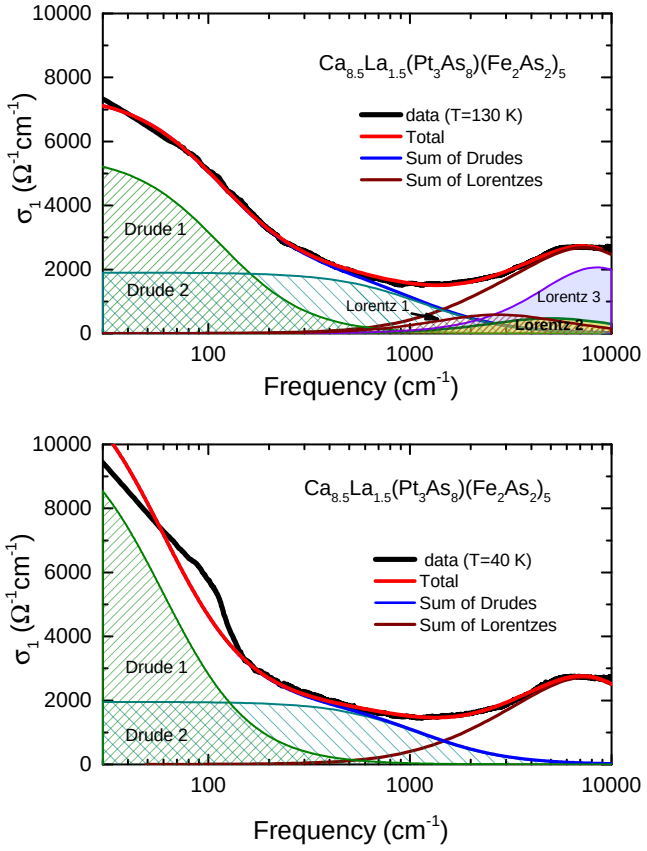

FIG. 6: (Color online) Typical Drude-Lorentz model fittings of the optical conductivity $\sigma_1(\omega)$ in the normal state: (A) 130 K data; (B) 40 K data. Both data were fitted with two Drude forms and three Lorentz oscillators. The Lorentz oscillator parts and Drude-2 form do not change much with temperatures, but the Drude-1 form becomes substantially sharpened with decreasing temperature.

Figure 6(A) shows that the 130 K data of $\sigma_1(\omega)$ and its Drude-Lorentz model fitting. It is well fitted with two Drude terms (one narrow and the other broad) and three Lorentz oscillator terms. Here two Drude terms show the presence of multiple bands in $Ca_{8.5}La_{1.5}(Pt_3As_8)(Fe_2As_2)_5$, as in many IBS compounds, e.g., LiFeAs compound[25]. The data of $\sigma_1(\omega)$ of 300 K and 240 K are also well fitted with the Drude-Lorentz model with the similar parameters: the spectral weights, $\omega^2_{p,j=1,2}$ and $S_{k=1,2,3}$, and the Lorentz oscillator frequencies $\omega_{L,k=1,2,3}$ are the same, but only the scattering rates, $\frac{1}{\tau_{D,j=1,2}}$ and $\frac{1}{\tau_{L,k=1,2,3}}$, need to be adjusted (see Fig.7).

However, the 40 K and 80 K data are different. While the Lorentzian part can be fitted as above only with the scattering rates $\frac{1}{\tau_{L,k=1,2,3}}$ adjusted, the low frequency Drude part has an extra hump structure around $\sim 100\ cm^{-1}$, as seen in Fig.3, hence can not be fitted by smooth Drude spectra. Nevertheless, it was shown in the previous section that the low frequency spectra of $\sigma_1(\omega;T)$ for $\omega < 1{,}000\ cm^{-1}$ separately conserve the spectral weight with temperature variation (see the pink inverse triangle data in Fig.4). Therefore, we tried to continue to use the same Drude-Lorentz model to fit the 40 K and 80 K data. Fig.6(B) shows the fitting result of the 40 K data. The Lorentzian part is fitted well as in the case of $T = 130$ K, confirming the separate sum rule, but the Drude part show a clear deviation. Comparing the experimental data (black solid line) and the model fitting (red solid line), it shows that the hump structure (extra spectral density) around $\omega \sim 100\ cm^{-1}$ is formed by draining a spectral density from the lower frequency part ($\omega < 50\ cm^{-1}$) of Drude spectra. This is a clear evidence that this hump structure is due to a partial gapping in the Drude spectra. If it were from an additional inter-band transition[27], then the lower frequency part of $\sigma_1(\omega)$ should have been fitted by a smooth Drude form – this was not possible with the sum rule satisfied. Impurity bound state scenario is also unrealistic because any potential scattering cannot form a bound state inside a Drude spectra without first forming a deep gap.

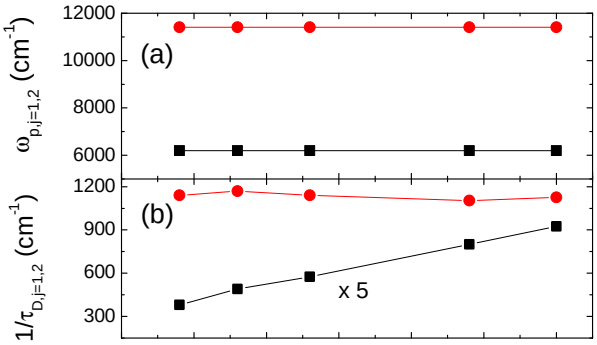

FIG. 7: (Color online) (a) The plasma frequency of the Drude bands, ω_{D1} (black solid square), and ω_{D2} (red solid circle). (b) The corresponding scattering rates, $1/\tau_{D1}$ (black solid square), and $1/\tau_{D2}$ (red solid circle).

In summary, (1) the spectral weight of the hump structure around $\omega \sim 100\ cm^{-1}$ is drained from the Drude spectra with a partial gapping in them; (2) this hump structure at 80 K and 40 K continuously evolve into the SC gap structure below T_c. We then conclude that the only remaining plausible scenario for the hump structure around $\omega \sim 100\ cm^{-1}$ is due to the preformed Cooper pairs. Fig.7 shows the temperature dependence of the fitting parameters of the Drude-Lorentz model fitting of the normal state optical conductivity $\sigma_1(\omega)$ from 40 K to 300 K.

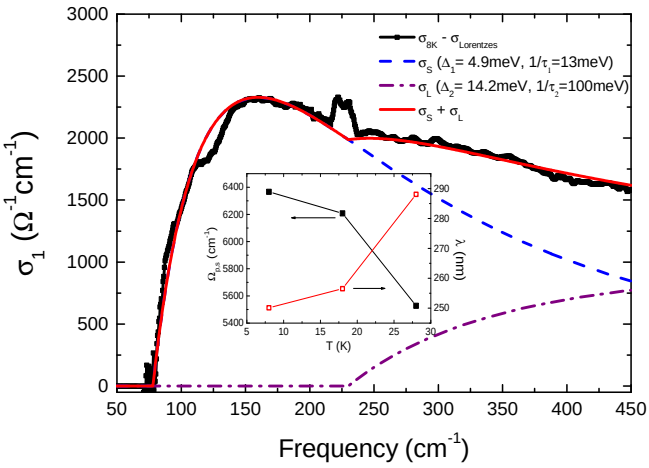

FIG. 8: (Color online) Mattis-Bardeen model fitting for the 8 K data (black solid line) of $\sigma_1^{exp}(\omega)$ after the Lorentz oscillator contribution subtracted. The data are decomposed into two Mattis-Bardeen terms (blue dashed line, and purple dash dotted line). The sum of the two Mattis-Bardeen terms is plotted as a red solid line. The inset represents the SC plasma frequency $\Omega_{p,S}(T)$ (black solid square) and the corresponding penetration depth $\lambda(T)$ (red open square).

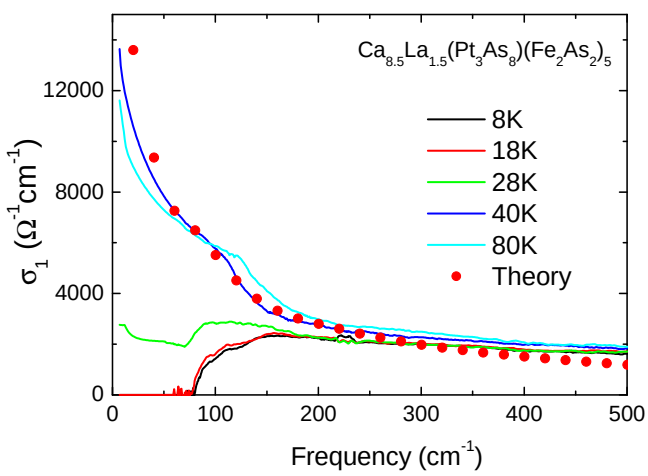

FIG. 9: (Color online) Theoretical calculation of $\sigma_1^{theo}(\omega, T > T_c)$ by the incoherent preformed Cooper pair model with $T = 40$ K, overlayed on the experimental data of $\sigma_1^{exp}(\omega, T)$ for T below and above $T_c = 32.8$ K.

D. $\sigma_1^{exp}(\omega; T < T_c)$ in the SC state

The three data set of $\sigma_1^{exp}(\omega; T < T_c)$ for T =8 K, 17 K, and 28 K, respectively, shown in Fig.3, clearly shows clean opening of a full gap, indicating an s-wave pairing. Combining with the presence of two Drude terms in the low frequency part of $\sigma_1^{exp}(\omega; T > T_c)$ in the normal state, as shown in the previous section, it is natural to assume two s-wave gaps in the SC state. Indeed, the line shape of the 8 K data (black solid line) of $\sigma_1^{exp}(\omega)$ appears to have two gaps with different sizes, Δ_1 and Δ_2. Therefore, we use the generalized Mattis-Bardeen formula for two band superconductor to fit the 8 K data of $\sigma_1(\omega)$. The spectral weight of two band and its scattering rate were taken as fitting parameters for optimal fitting, but those values turn out to be quite consistent with the values of the normal state Drude terms, $\omega^2_{p,j=1,2}$ and $1/\tau_{D,j=1,2}$. The results are shown in Fig.8.

The black solid line in Fig. 8 shows the SC optical conductivity after subtracting the Lorentz oscillator contribution at high frequencies, which is almost independent of temperature, from the optical conductivity of 8 K. The data shows the absorption edge at about 80 cm^{-1}, proportional to the first SC gap ($\sim 2\Delta_1$), and a weak kink at about 220 cm^{-1} indicating a second SC gap ($\sim 2\Delta_2$). With the generalized Mattis-Bardeen model, the SC gap sizes (the scattering rates) were determined to be Δ_1 = 4.9 meV ($1/\tau_1 = 13.1$ meV) and Δ_2 = 14.2 meV ($1/\tau_2 = 37.1$ meV), respectively. The ratios of gap magnitude to T_c, $R = 2\Delta/k_BT_c$, were evaluated as 3.6 and 10.2, respectively. The average value of R, being much larger than $R_{BCS} = 3.5$, implies that the superconductivity in $Ca_{8.5}La_{1.5}(Pt_3As_8)(Fe_2As_2)_5$ belongs to a strong coupling limit. The relative sizes of the plasma frequency (spectral weight) of each band are 2 (small gap band) to 1 (large gap band), consistent with the normal state Drude weights of two band. This overall "inverse" relation – the smaller gap band carries a larger spectral weight and a weaker scattering rate while the larger gap band carries a smaller spectral weight and a stronger scattering rate – is consistent with the $s^{\pm}$-wave pairing scenario, which is mediated by a dominant interband scattering[25, 32].

In the inset, we also calculated the condensation strength from the missing spectral weight (the SC plasma frequency $\Omega_{p,S}(T)$) and the corresponding penetration depth $\lambda(T)$ using the London formula $\Omega^2_{p,S}(T) = c^2/\lambda^2(T)$.

E. $\sigma_1^{exp}(\omega; T_c < T \leq 80\ K)$: Pseudo Gap and Preformed Cooper Pair Model

In order to understand the data of $\sigma_1^{exp}(\omega, T)$ above T_c but below 80 K, we adopted the phase incoherent preformed Cooper pair model [33]. In the ordinary SC state below T_c, the real part of the optical conductivity is calculated by a standard Kubo formula with sum of two bands ($a = 1, 2$) as follows,

$$\sigma_1(\omega, T) = -\frac{\sum_a Im\Lambda_{a,xx}(\omega)}{\omega} \quad (3)$$

with

$$Im\Lambda_{a,xx}(\omega) = \pi e^2 \int d^2k d\omega' v^2_{a,x}(k) \times Tr[\bar{A}_a(k, \omega+\omega')\bar{A}_a(k, \omega')][f(\omega+\omega') - f(\omega)] \quad (4)$$

where $f(\omega)$ is the Fermi-Dirac distribution function, and $v_{a,x}$ is the Fermi velocity along the x-direction of the quasiparticles of the band "a". And $\bar{A}_a(k,\omega)$ is the 2×2 spectral density matrix of Nambu green's function of the band "a" in the SC state defined as $\bar{A}_a(k,\omega) = -Im\bar{G}_a(k,\omega)/\pi$ with

$$\bar{G}_a(k,\omega) = \frac{\tilde{\omega}\tau_0 + \xi_a(k)\tau_3 + \Delta_a\tau_1}{\tilde{\omega}^2 - \xi_a^2(k) - \Delta_a^2} \quad (5)$$

where Δ_a is the SC gap of the band "a" and τ_i are Pauli matrices. The damping rate Γ_a is included in $\tilde{\omega} = \omega + i\Gamma_a$ to fit the overall line shape, and in the extreme dirty limit such as $\Gamma_a \gg \Delta_a$, the total conductivity formula Eq.(3) reduces to the generalized Mattis-Bardeen formula[31]. Without knowing $v_{a,x}$, the combined factor $v_{a,x}^2 \int d^2k$ are taken as the parameter of the relative spectral weight of the each band $N_{a=1,2}^0$.

To simulate the phase fluctuations, we followed the recipe of Franz and Millis [34] and averaged the Nambu green's function Eq.(5) with Doppler shift energy η in the quasiparticle excitations as

$$\tilde{\bar{G}}(k,\omega) = \int d\eta P(\eta)\bar{G}(k,\omega-\eta) \quad (6)$$

where the probability distribution of η is given by $P(\eta) = \sqrt{2\pi W}e^{-\eta^2/2W}$ with $W \approx 3.48\alpha_v(T/T_c)\Delta^2$. α_v is a parameter derived from the XY-model and was estimated ≈ 0.009 in the high-T_c cuprates by Franz and Millis [34], for example.

Here, we take the whole W as a fitting parameter and chose $W_a = 0.06\Delta_a^2$, which corresponds to $T \approx 1.4T_c$, for the best fitting of the 40 K optical conductivity data. The results are plotted in Fig.9 by open red circle symbols. We used the same gap values of $\Delta_1 = 4.9$ *meV* and $\Delta_2 = 14.2$ *meV* of Mattis-Bardeen model fitting in the SC state for 8 K data, and adjusted the scattering rates as $1/\tau_1 = 13$ *meV* and $1/\tau_2 = 100$ *meV*, with cutoffs for $\omega < 2\Delta_{a=1,2}$, respectively. The overall fitting is reasonably good and, in particular, it demonstrates that the hump structure around 100 cm^{-1} is qualitatively and quantitatively reproduced by the fluctuations of the incoherent SC OP $\Delta_{a=1,2}$.

IV. CONCLUSIONS

We have measured the optical reflectivity $R(\omega,T)$ of the optimally doped $Ca_{8.5}La_{1.5}(Pt_3As_8)(Fe_2As_2)_5$ single crystal (T_c = 32.8 K) for frequencies from 40 cm^{-1} to 12,000 cm^{-1} and for temperatures from 8 K to 300 K. In the normal state for T = 130 K, 240 K, and 300 K, the optical conductivity data $\sigma_1(\omega,T)$ are well fitted by the Drude-Lorentz model with two Drude forms and three Lorentz oscillators. We have also found that (1) despite a huge variation of the spectral weight redistribution with temperature variation, the f-sum rule is satisfied; (2) also, divided by $\omega^* \sim 1{,}000\ cm^{-1}$, the spectral weights above and below ω^* are separately conserved, which suggests that the original bare conduction electrons are split into the low energy itinerant carriers (Drude spectra) and the high energy localized carriers (Lorentzian oscillators) due to the strong correlation effects.

In the SC state for T = 28 K, 17 K, and 8 K, the $\sigma_1(\omega, T < T_c)$ data show a clean gap opening at $\sim 80\ cm^{-1}$ and the second gap structure at $\sim 220\ cm^{-1}$. The $\sigma_1(\omega, T = 8\ K)$ data is well fitted with two SC gaps, $\Delta_1 = 4.9$ *meV* and $\Delta_2 = 14.2$ *meV*, consistent with the presence of two Drude bands observed in the normal state data. From the estimated fraction of the condensate spectral weight below T_c, we have estimated that only about 29% of the conduction band carriers participates in the SC condensation indicating that $Ca_{8.5}La_{1.5}(Pt_3As_8)(Fe_2As_2)_5$ is in dirty limit.

Most interestingly, the $\sigma_1(\omega, T = 40, 80\ K)$ data, in the intermediate temperature region above T_c but below $\sim$ 80 K, showed a PG-like hump structure at the exactly same energy scale as the SC gap energy on top of the smooth Drude-like spectra. We have demonstrated that this PG-like hump structure can be consistently fitted with the preformed Cooper pair model using the same SC gap values of $\Delta_{1,2}$ of the SC state. Our work showed that the optimally doped $Ca_{8.5}La_{1.5}(Pt_3As_8)(Fe_2As_2)_5$ is a multigap superconductor having a clear PG formed by incoherent preformed Cooper pairs up to 80 K (about three times of T_c), therefore added one more case to the list of the IBSs with the PG due to the SC correlation[21, 22].

V. ACKNOWLEDGMENTS

YSK was supported by the NRF grant 2015M2B2A9028507 and 2016R1A2B4012672. YKB was supported by NRF Grant 2016-R1A2B4-008758.

[1] N. Ni, J. M. Allred, B. C. Chan, and R. J. Cava, Proc. Natl. Acad. Sci. **108**, 45 (2011)
[2] S. Kakiya, K. Kudo, Y. Nishikubo, K. Oku, E. Nishibori, H. Sawa, T. Yamamoto, T. Nozaka, and M. Nohara, J. Phys. Soc. Jpn. **80**, 093704 (2011)
[3] T. Sturzer, G. Derondeau, and D. Johrendt, Phys. Rev. B **86**, 060516 (2012)
[4] A. Sapkota, G. S. Tucker, M. Ramazanoglu, W. Tian, N. Ni, R. J. Cava, R. J. McQueeney, A. I. Goldman, and A. Kreyssig, Phys. Rev. B **90**, 100504 (2014)
[5] C. Loehnert, T. Sturzer, M. Tegel, R. Frankovsky, G. Friederichs, and D. Johrendt, Angew. Chem. Int. Ed. **50**, 9195 (2011).
[6] T. Sturzer, G. M. Friederichs, H. Luetkens, A. Amato, H. H. Klauss, F. Winter, R. P?ttgen, and D. Johrendt, J. Phys.: Condens. Matter **25**, 122203 (2013).
[7] K. Haule, J. H. Shim, and G. Kotliar, Phys. Rev. Lett. **100**, 226402 (2008)
[8] I. R. Shein and A. L. Ivanovskii, arXiv:1108.0495 (2011)
[9] S. Thirupathaiah, T. Sturzer, V. B. Zabolotnyy, D. Johrendt, B.

Buchner, and S. V. Borisenko, Phys. Rev. B **88**, 140505 (2013)
[10] N. Ni, W. E. Straszheim, D. J. Williams, M. A. Tanatar, R. Prozorov, E. D. Bauer, F. Ronning, J. D. Thompson, and R. J. Cava, Phys. Rev. B **87**, 060507 (2013)
[11] P. Gao , L. Sun , N. Ni , J. Guo , Q. Wu , C. Zhang , D. Gu , K. Yang , A. Li , S. Jiang , R. J. Cava , and Z. Zhao, Adv. Mater. **26**, 2346 (2014)
[12] M. Neupane, C. Liu, S. Y. Xu, Y. J. Wang, N. Ni, J. M. Allred, L. A. Wray, N. Alidoust, H. Lin, R. S. Markiewicz, A. Bansil, R. J. Cava, and M. Z. Hasan, Phys. Rev. B **85**, 094510 (2012)
[13] J. Kim, F. Ronning, N. Haberkorn, L. Civale, E. Nazaretski, N. Ni, R. J. Cava, J. D. Thompson, and R. Movshovich, Phys. Rev. B **85**, 180504 (2012)
[14] E. Mun, N. Ni, J. M. Allred, R. J. Cava, O. Ayala, R. D. McDonald, N. Harrison, and V. S. Zapf, Phys. Rev. B **85**, 100502 (2012)
[15] T. Zhou, G. Koutroulakis, J. Lodico, N. Ni, J. D. Thompson, R. J. Cava and S. E. Brown, J. Phys.: Condens. Matter **25**, 122201 (2013)
[16] K. Cho, M. A. Tanatar, N. Ni and R. Prozorov, Supercond. Sci. Technol. **27**, 104006 (2014)
[17] Y. Kamihara, T. Watanabe, M. Hirano, and H. Hosono, J. Am. Chem. Soc. **130**, 3296 (2008)
[18] X. H. Chen, T. Wu, G. Wu, R. H. Liu, H. Chen, and D. F. Fang, Nature. **453**, 761 (2008)
[19] Z. A. Ren, G. C. Che, X. L. Dong, J. Yang, W. Lu, W. Yi, X. L. Shen, Z. C. Li, L. L. Sun, F. Zhou, Europhys. Lett. **83**, 17002 (2008)
[20] F. C. Hsu, J. Y. Luo, K. W. Yeh, T. K. Chen, T. W. Huang, P. M. Wu, Y. C. Lee, Y. L. Huang, Y. Y. Chu, D. C. Yan, and M. K. Wu, Proc. Natl. Acad. Sci. **105**, 38 (2008)
[21] Y. S. Kwon, J. B. Hong, Y. R. Jang, H. J. Oh, Y. Y. Song, B. H. Min, T. Iizuka, S. Kimura, A. V. Balatsky, and Y. Bang, New J. Phys. **14**, 063009 (2012)
[22] Y. M. Dai, B. Xu, B. Shen, H. H. Wen, J. P. Hu, X. G. Qiu, and R. P. S. M. Lobo, Phys. Rev. B **86**, 100501 (2012)
[23] R. P. S. M. Lobo, Y. M. Dai, U. Nagel, T. Room, J. P. Carbotte, T. Timusk, A. Forget, and D. Colson, Phys. Rev. B **82**, 100506 (2010)
[24] M. A. Surmach, F. Bruckner, S. Kamusella, R. Sarkar, P. Y. Portnichenko, J. T. Park, G. Ghambashidze, H. Luetkens, P. K. Biswas, W. J. Choi, Y. I. Seo, Y. S. Kwon, H.-H. Klauss, and D. S. Inosov, Phys. Rev. B **91**, 104515 (2015)
[25] B. H. Min, J. B. Hong, J. H. Yun, T. Iizuka, S. Kimura, Y. Bang, and Y. S. Kwon, New J. Phys. **15**, 073029 (2013)
[26] Y. M. Dai, B. Xu, B. Shen, H. Xiao, H. H. Wen, X. G. Qiu, C. C. Homes, and R. P. S. M. Lobo, Phys. Rev. Lett. **111**, 117001 (2013)
[27] E. van Heumen, Y. Huang, S. de Jon, A.B. Kuzmenko, M.S. Golden, and D. van der Marel, Europhys. **90**, 37005 (2010).
[28] F. Carbone, A. B. Kuzmenko, H. J. A. Molegraaf, E. Heumen, E. Giannini, and D. Marel, Phys. Rev. B **74**, 024502 (2006)
[29] R. A. Ferrell, and R. E. Glover III, Phys. Rev. **109**, 1398 (1958)
[30] M. Tinkham, and R. A. Ferrell, Phys. Rev. Lett. **2**, 331 (1959)
[31] W. Zimmermann, E. H. Brandt, M. Bauer, E. Seider, and L. Genzel, Physica C **183**, 99 (1991)
[32] Y.K. Bang and H.Y. Choi, Phys. Rev. B **78**, 134523 (2008).
[33] V. J. Emery and S. A. Kivelson, Nature **374**, 434 (1995).
[34] M. Franz and A. J. Millis, Phys. Rev. B **58** 14572 (1998).